

Topical Review

Recent progress of scanning tunneling microscopy/spectroscopy study of Majorana bound states in the $\text{FeTe}_{0.55}\text{Se}_{0.45}$ superconductor

Geng Li^{1,2,3,4} , Shiyu Zhu^{1,2} , Dongfei Wang^{1,2,6}, Yeliang Wang^{1,5}
and Hong-Jun Gao^{1,2,3,4,*} 

¹ Institute of Physics, Chinese Academy of Sciences, Beijing 100190, People's Republic of China

² School of Physical Sciences, University of Chinese Academy of Sciences, Beijing 100190, People's Republic of China

³ CAS Center for Excellence in Topological Quantum Computation, University of Chinese Academy of Sciences, Beijing 100190, People's Republic of China

⁴ Songshan Lake Materials Laboratory, Dongguan, Guangdong 523808, People's Republic of China

⁵ School of Information and Electronics, MIT Key Laboratory for Low-Dimensional Quantum Structure and Devices, Beijing Institute of Technology, Beijing 100081, People's Republic of China

⁶ Department of Physics, University of Hamburg, 20355 Hamburg, Germany

E-mail: hjgao@iphy.ac.cn

Received 21 December 2020, revised 22 February 2021

Accepted for publication 11 May 2021

Published 4 June 2021



CrossMark

Abstract

Majorana bound states (MBSs) are spatially-localized zero-energy quasiparticles following non-Abelian braiding statistics that hold a great promise for fault-tolerant topological quantum computing. Different platforms have been designed to realize the MBSs in condensed matter, including semiconducting nanowire in proximity to conventional superconductors, superconductor-topological insulator layered heterostructures, 1D atomic chains on superconducting surface. Recently, iron-based superconductors have emerged as a new platform for studying Majorana zero mode. A sharp zero-bias peak inside a vortex core that does not split when moving away from the center is observed by scanning tunneling microscopy (STM) in $\text{FeTe}_{0.55}\text{Se}_{0.45}$. This zero-energy mode is assigned to the MBS. In this topic review, we present an overview of the recent experimental works of STM studies on the MBS. We start with the STM identification of MBSs in the vortices in $\text{FeTe}_{0.55}\text{Se}_{0.45}$ and discuss the advantages $\text{FeTe}_{0.55}\text{Se}_{0.45}$ compared with other platforms. We then review the topological origin of the MBS and discuss the reason why the MBS is not seen in every single vortex. We also review the recently observed nearly quantized conductance plateau feature of the MBS owing to its particle–antiparticle equivalence. Finally, we give perspective on future experimental works in this field, where the next important steps towards braiding of MBS can be expected.

* Author to whom any correspondence should be addressed.

Keywords: STM/S, FeTe_{0.55}Se_{0.45}, Majorana bound states, Majorana zero mode, topological surface states

(Some figures may appear in color only in the online journal)

1. Introduction

A Majorana fermion is a fermion whose antiparticle is itself [1]. This can be written mathematically as $\gamma^\dagger = \gamma$ if we define the Majorana fermion annihilation operators γ_1, γ_2 with the corresponding electron creation and annihilation operator c^\dagger, c as follows: $\gamma_1 = (c + c^\dagger)/\sqrt{2}$ and $\gamma_2 = -i(c - c^\dagger)/\sqrt{2}$. The search for Majorana fermion dates back to the early days of relativistic quantum mechanics. However, the elementary Majorana fermions have never been observed by particle physicists. In condensed matter we can construct charge neutral quasiparticle excitations with particle and anti-particle symmetry, which are usually bound states having zero energy called Majorana zero modes (MZMs) [2–4]. The braiding of two MZMs follows non-Abelian statistics [4–6]. During the braiding process, the MZMs are topologically protected from any local perturbation and can be used in fault-tolerant quantum computation [7–10].

The realization of unpaired MZM relies on two conditions: (a) particle–hole symmetry must be conserved. (b) The spin of the quasiparticle must be the same under a charge conjugate transformation. A natural platform which satisfies the first condition is the superconductors, where quasiparticles are superpositions of electrons and holes. However, the realization of the second condition is highly non-trivial. As we all know, the conventional BCS superconductors usually have a s-wave pairing between the electrons. The wavefunction of simplest excitation in such superconductor can be written as: $\psi = \frac{1}{\sqrt{2}} (c_\uparrow^\dagger + c_\downarrow) |0\rangle$ where the arrows represent spin and $|0\rangle$ represents the vacuum. Under a charge conjugate transformation, $\psi^c = \frac{1}{\sqrt{2}} (c_\downarrow^\dagger + c_\uparrow) |0\rangle$ which is no longer the initial wave function. ψ can be a charge conjugate transformation invariant if the superconductor is spinless or fully spin polarized.

In 1990, Moore and Read first realized the ‘Pfaffian’ trial wavefunctions for fractional quantum Hall state could support non-Abelian anyons [11]. Later on, Read and Green proved that the weak pairing spinless 2D p-wave superconductor has a pair wave function that is asymptotically the same as that in the Moore–Read Pfaffian quantum Hall state [12]. This led to a conclusion that the universal properties of the Pfaffian state such as non-Abelian statistics must also be shared by the p-wave superconductor. For an infinite 2D p-wave superconductor, one can create a topological defect by adding magnetic flux quantum on the surface. The MZM is expected to appear at the center of the vortex. Ivanov [5] demonstrated that a half-quantum vortex for spinful fermions is equivalent to a single quantum vortex in a p-wave superconductor of spinless fermions. Kitaev [13] further discussed the possibility of unpaired Majorana fermions appearing at the ends of 1D quantum wire.

However, superconductor with p-wave pairing is rare in nature. A more realistic model was proposed by Fu and Kane in 2008 by taking advantage of the surface states of 3D topological insulators [14]. It was shown that under a unitary transformation, an effective p-wave pairing can be achieved, and the MZM could be found at the vortex core. On the other hand, Lutchyn *et al* showed that MZMs can also be realized based on semiconductor–superconductor heterostructures [15, 16]. The effective p-wave pairing was achieved by engineering Rashba band of the semiconductor with proper parameters of chemical potential, Zeeman field, superconducting gap and spin–orbit coupling (SOC) strength. Bernevig *et al* further showed that topological nontrivial phase can be achieved by using magnetic non-collinear structures proximately by an s-wave superconductor in both 1D [17–20] and 2D [21]. The topology of the Shiba bands of the magnetic adsorbates can be engineered by tuning parameters including SOC amplitude, magnetic exchange coupling amplitude and chemical potential. More recently, the planar Josephson junction hosting two-dimensional electron gas with strong SOC was also predicted to be a good platform to study Majorana bound state (MBS) [22]. With a phase difference of π between the two superconducting leads, the topological phase is obtained at almost any value of the Zeeman field and chemical potential.

Following these predictions, several systems have been experimentally proved as promising platforms for detecting MZMs in the past decade. Large SOC 1D semiconducting nanowires [23–27], 1D magnetic atomic chains [14, 28–31], 2D gold thin films [32, 33], 2D planar Josephson junctions [34, 35] and 3D topological insulators [36, 37], in proximity with an s-wave superconductor, have been reported to support MBSs. Progress has been made by identifying MZMs in above systems [27, 28, 36]. MZM was also observed at the boundary of magnetic island made of Co [38], Fe [39] and more recently CrBr₃ [40]. However, the material/device fabrication process and the detection of MZM are still challenging. For example, it is difficult to make clean interfacial contacts with the superconductor in the semiconducting nanowire system. Also, the experiments need to be operated under very low temperatures since a long superconducting coherent length is required. Therefore, new platforms need to be explored to overcome these drawbacks.

In 2018, Zhang *et al* observed a spin-momentum locking pattern of the Dirac surface band, an hallmark of a topological insulator, in FeTe_{0.55}Se_{0.45} [41]. This Dirac surface band opens a superconducting gap below the bulk T_c , which is identical to the interfacial state in the Fu–Kane model [42]. This result quickly attracts interests in the field since the system has a reasonably high T_c and is as simple as a single piece of bulk material. This material is referred to as connate topological

superconductors in some studies [43], which is believed to be a good platform to observe MZMs.

The following up scanning tunneling microscopy/spectroscopy (STM/S) experiments on $\text{FeTe}_{0.55}\text{Se}_{0.45}$ by Wang *et al* indeed show signatures of a spatial non-split zero-bias peak (ZBP), which is further determined as a fingerprint of the MBS [44]. Recently, Zhu *et al* observed the nearly quantized conductance plateau of the ZBP using a variable-tunnel-coupling technique and gave strong evidence to the MBS in the same material [45]. Wang *et al* reported observation of dispersing 1D Majorana channels at the domain wall in $\text{FeTe}_{0.55}\text{Se}_{0.45}$ [46]. Chen *et al* reported zero-energy end states at the atomic line defects in monolayer $\text{FeTe}_{0.5}\text{Se}_{0.5}$ grown on $\text{SrTiO}_3(001)$ substrate [47]. Also, evidence of MBSs in other iron-based superconductors [48] has been reported.

In this review, we will focus on the STM/S studies on the MBSs in $\text{FeTe}_{0.55}\text{Se}_{0.45}$. We first review the experimental observation of the MBS in the vortex cores of $\text{FeTe}_{0.55}\text{Se}_{0.45}$ in section 2. Then we discuss the physical origin of two different types of vortices in section 3 and create relation between the MBS and the topological surface states. In section 4 we review a recent work revealing the nearly quantized conductance plateau of the MBS. In the last two sections we will talk about some other topologically non-trivial platforms feasible for STM study and give a perspective on future work that STM can be potentially used in Majorana research.

2. Discovery of MBS in $\text{FeTe}_{0.55}\text{Se}_{0.45}$

2.1. Topologically non-trivial band structure of $\text{FeTe}_{0.55}\text{Se}_{0.45}$

In 2015, the topological non-trivial band structure of $\text{FeTe}_{0.55}\text{Se}_{0.45}$ was discovered by Wang *et al* [49]. The Te substitution enhances the hopping between neighboring layers, and consequently a band inversion occurs at Γ -Z line compared to FeSe. Soon after, a full phase diagram was given by Xu *et al* [50] which shows $\text{FeTe}_{0.55}\text{Se}_{0.45}$ without gating is actually within the topological non-trivial regime.

Up to now, while some works presented results indicating the trivial origin of the band structure of $\text{FeTe}_{0.55}\text{Se}_{0.45}$ [51, 52], more and more studies support the existence of the topological surface state [41, 44, 45, 53]. The discrepancy of experimental results is likely due to the narrow topological window and the well-known inhomogeneity [46, 54] of the electronic structure of the material. ARPES observation [41] of $\text{FeTe}_{0.55}\text{Se}_{0.45}$ surface shows a Dirac-cone like feature near the Fermi level. The Dirac-cone has a spin helical structure, suggesting that the surface state of $\text{FeTe}_{0.55}\text{Se}_{0.45}$ is topologically non-trivial. Therefore, once the temperature is below T_c , the surface of $\text{FeTe}_{0.55}\text{Se}_{0.45}$ will become topological superconducting. The MBS which shows up at zero energy is expected to appear at the center of vortex core.

2.2. Zero-energy mode at the vortex center

Based on the theoretical proposal and the ARPES results, Wang *et al* carried out STM investigations of on the surface

of $\text{FeTe}_{0.55}\text{Se}_{0.45}$ [44]. The surface Te/Se atoms can be identified from high resolution STM image (figure 1(a)), showing inhomogeneous distribution of Te/Se atoms. Scanning tunneling spectroscopy (STS) in figure 1(b) shows good agreement in the band features with previous ARPES results. After application of a magnetic field perpendicular to the sample surface, the Abrikosov vortex can be resolved in the differential conductance maps taken at zero energy (figure 1(c)). The differential conductance map shows highest intensity at the vortex center and gradual decay in intensity away from the center. Detailed STS linecut map and waterfall plot are shown in figures 1(d) and (e). A pronounced and robust ZBP can be resolved from the spectrum taken at the vortex center, and it does not split away from the vortex center. This behavior is different from Caroli-de Gennes-Matricon bound states (CBSs) [55, 56] in the non-quantum limit which show a splitting of zero energy when moving from vortex center to the boundary. The $\text{FeTe}_{0.55}\text{Se}_{0.45}$ system has a large Δ/E_F ratio, giving rise to a large separation between the ZBP and the first level CBS. As a result, the ZBP can be regarded as a ‘clean’ Majorana mode, which benefits further in-depth investigations as will be elaborated in section 3.

2.3. Magnetic field and temperature dependence of MBS

Magnetic field dependent and temperature dependent experiments have been carried out to rule out the topologically trivial origins of this ZBP. Figures 2(a) and (b) show that this zero-energy mode is stable under high magnetic field up to 6 T, which rule out the possibility of Kondo effect. Other phase sensitive origins such as weak-anti localization effect and coherent Andreev reflection can also be ruled out as high magnetic field will destroy the phase conjugation. Therefore, this zero-energy mode is assigned to MBS which has a topologically non-trivial origin. Temperature dependent experiments show that the MBS will disappear once the temperature exceed 3 K (figure 3(a)). This behavior is repeated in different vortices as shown in figure 3(b).

It has been pointed out by previous theoretical studies [50, 57, 58] that the condition of a bulk vortex line, such as its chemical potential, has substantial influences on the Majorana mode on the surface by the vortex phase transition. As the bulk band structure is trivial, traditional CBSs will appear inside the vortex line. When the temperature is low, CBSs are well separated from each other and the MBS at the end of the vortex line is well protected by the gap. However, when the temperature ramps up, the thermo broadening effect will smear the CBSs and there will be no gap protecting the MBS. Quasiparticles near zero-energy will strongly interact with (or poison) the MBS. As a result, the ZBP will be strongly suppressed at elevated temperatures (>3 K) (figures 3(c) and (d)).

2.4. Discussion

While the zero-energy peak has been identified as MBS, there are still some open questions left to be solved. In the experiment, it is found that some vortices show only trivial CBSs without zero energy peak even within the same field of view

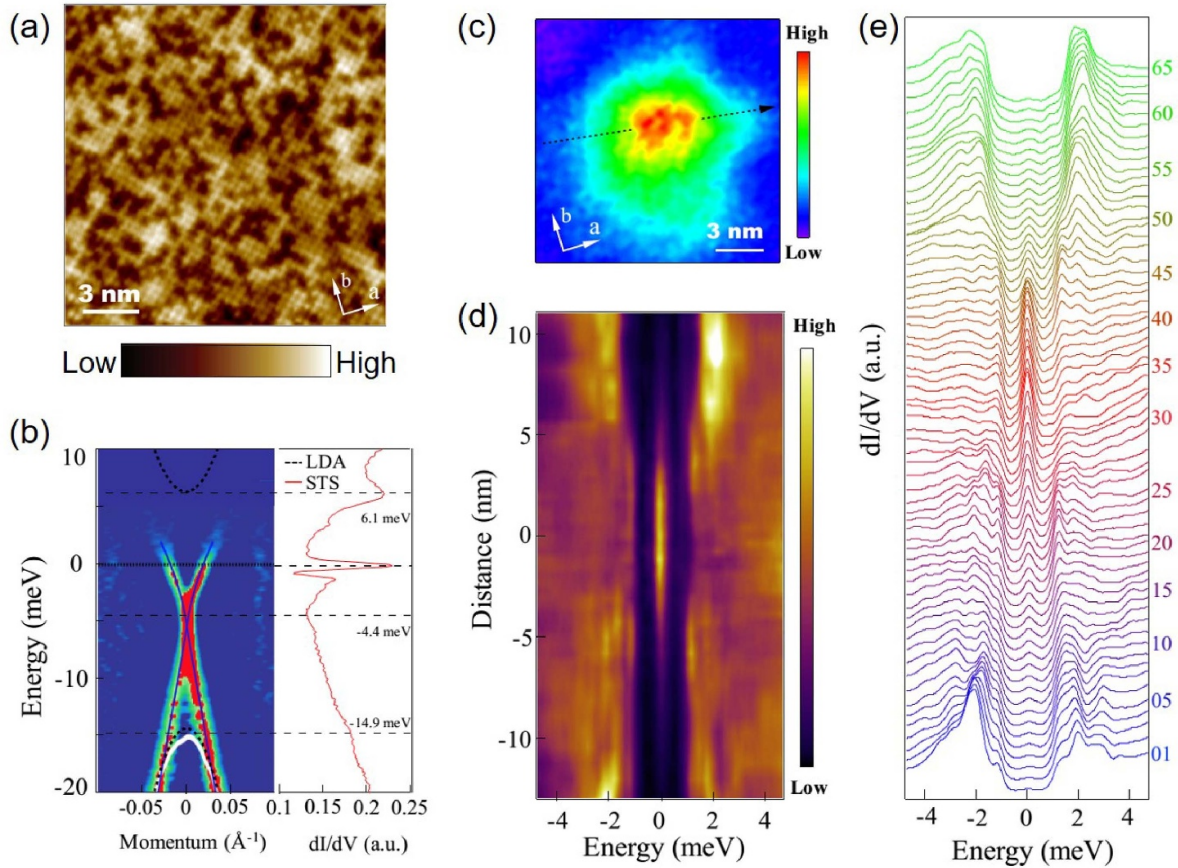


Figure 1. MBSs in the vortex core of $\text{FeTe}_{0.55}\text{Se}_{0.45}$. (a) STM topography of $\text{FeTe}_{0.55}\text{Se}_{0.45}$. (b) Comparison between ARPES and STS results. (c) A zero-bias conductance map around vortex core. (d) A line-cut intensity plot along the black dashed line in (c). (e) A waterfall-like plot of (d) with 65 spectra, with the black curve corresponding to the one in the core center. From [44]. Reprinted with permission from AAAS. All rights reserved.

where other vortices host MBSs. The existence of these trivial vortices is attributed to regions that do not have topological surface state, which is likely due to the inhomogeneous chemical potential on $\text{FeTe}_{0.55}\text{Se}_{0.45}$ surface, and will be discussed in detail in section 3.

Another question is that the chance to find vortices hosting MBS varies under different magnetic field. Machida *et al* [59] found that the fraction of vortices hosting MBSs decreases with increasing magnetic field. Moreover, they showed that local quenched disorders are not related to the MBSs. Recent theoretical calculation [60] reveals that the Majorana hybridization and disordered vortex distribution are responsible for the decreasing fraction of the ZBPs observed in the experiment.

3. Half-integer level shift of vortex bound states in $\text{FeTe}_{0.55}\text{Se}_{0.45}$

Following the discussion in the last section, while a non-shift ZBP across the vortex core is regarded as a strong indication of MZM and topological nature of the superconducting vortex [36, 42, 44, 48], the observation of ZBPs only appear in part of the vortices on an $\text{FeTe}_{0.55}\text{Se}_{0.45}$ surface, which has been confirmed by other independent research groups [51]. Moreover,

these two kinds of vortices seem to exist together in an area on $\text{FeTe}_{0.55}\text{Se}_{0.45}$ surface.

In order to demonstrate the physics behind those two classes of vortices, it is important to further study the spectroscopic difference between them. Based on that, the two types of vortices are classified as topological vortex (which hosts an ZBP in the center) and ordinary vortex (which has only CBSs). This phenomenon reveals another character of $\text{FeTe}_{0.55}\text{Se}_{0.45}$ and make it a good platform to demonstrate the fundamental distinction between the two classes of vortices, which differ not only by the presence or absence of ZBP, but also by quantization sequence of the remaining higher energy sub-gap states and their spatial pattern [61].

3.1. Topological vortex cores with integer quantized CBSs

As has been discussed in section 2.2, the non-split and non-shift sharp ZBP in the center of a topological vortex core (figures 1(c) and 4(a)) has been assigned to the MBSs. Depending on the local Δ/E_F value, other in-gap states, the CBSs (figures 4(b) and (c)) [55], appear in some of the vortices, which are crucial in determining the topological nature of the vortices [61]. Figures 5(a) and (b) show the line-cut through a topological vortex with an MBS at the center. The large

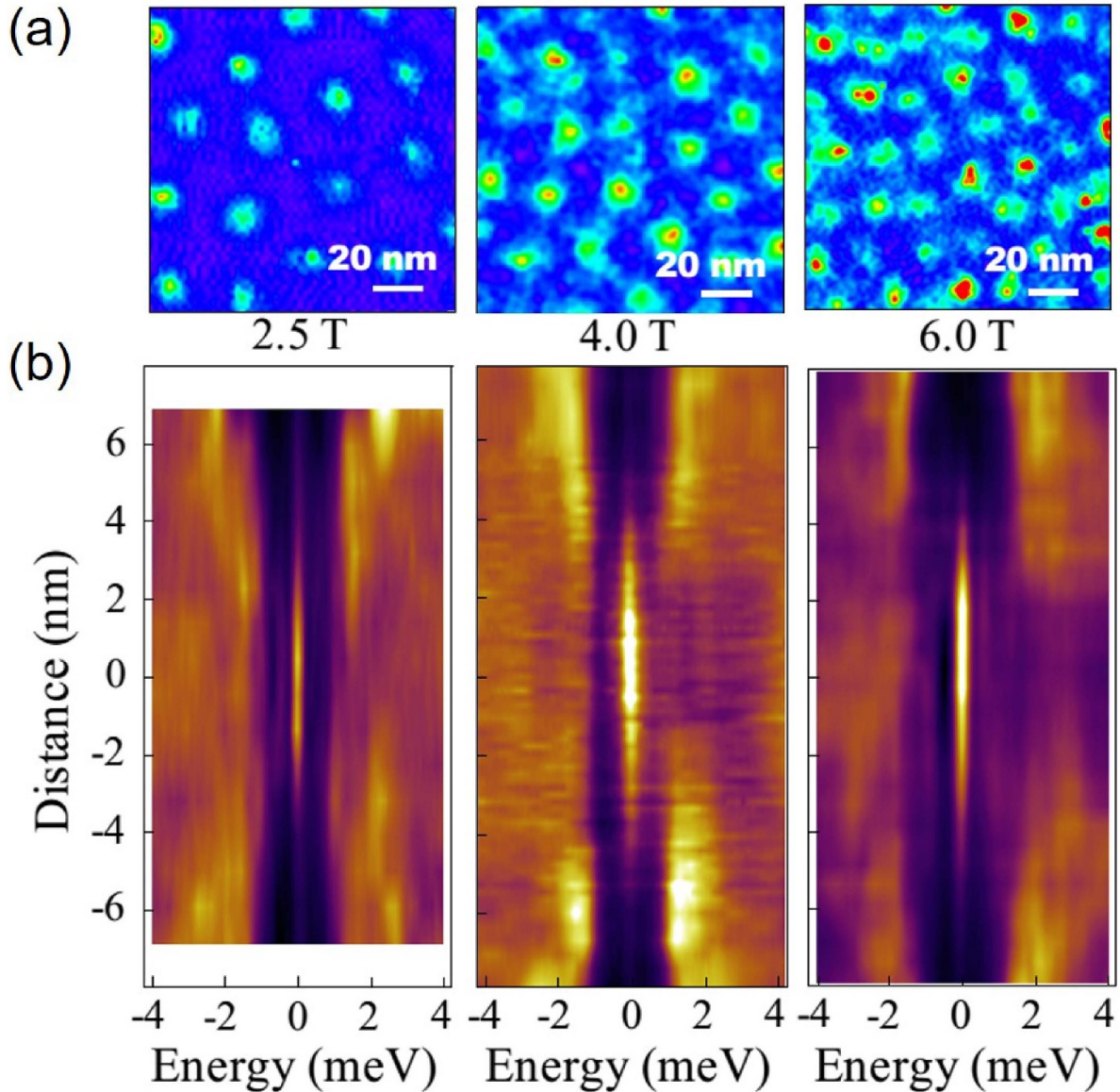


Figure 2. Magnetic field dependence of MBSs. (a) $120\text{ nm} \times 120\text{ nm}$ ZBC maps at 2.5 T, 4.0 T, and 6.0 T, respectively. (b) Line-cut intensity plots at 2.5 T, 4.0 T, and 6.0 T, respectively. From [44]. Reprinted with permission from AAAS. All rights reserved.

ratio [44, 62] of Δ/E_F enables detection of the quantum limit [63], where the CBSs also appear as discernible non-shift discrete energy levels in the dI/dV spectra. These bound states are almost equally spaced in energy. The CBSs can be also visualized in an overlap plot, with several spatially non-shifting peaks coexisting with the sharp MZM as shown in figure 5(c). By using the energy of the first level as the energy unit, the energy levels show the ratio $(E_L/\Delta E)$ in the form of 0:1:2:3, which is an integer quantized sequence. Although the absolute level energies vary slightly from vortex to vortex, the integer quantized sequence is always valid as shown in figure 5(d).

3.2. Ordinary vortex cores with half-odd-integer quantized CBSs

The other type of vortex is topologically trivial and is therefore called the ordinary vortex. A typical example is shown

in figures 6(a)–(c). Different from the topological vortex, the ordinary vortex does not have an ZBP at the center. Moreover, the energy levels follow the sequence of 0.5:1.5:2.5:3.5:4.5 (figure 6(d)). These CBSs show a strong particle–hole asymmetry, which is a common phenomenon at the superconducting vortex core in iron-based superconductors [64, 65].

The observation of quantized CBSs energy levels in two types of vortices reveal their intrinsic difference in the topological nature. In an ordinary vortex core (figure 7(a)), only the conventional bulk bands contribute to the low energy quasiparticle excitations [61]. Accordingly, the energy eigenvalues of CBSs are approximately half-odd-integer quantized, i.e. $E_\nu = \nu\Delta^2/E_F$ ($\nu = \pm 1/2, \pm 3/2, \pm 5/2, \dots$), with ν being the eigenvalue of angular momentum [55, 63, 66]. On the other hand, the angular momentum in topological vortices (figure 7(b)) gain an additional half-odd-integer contribution

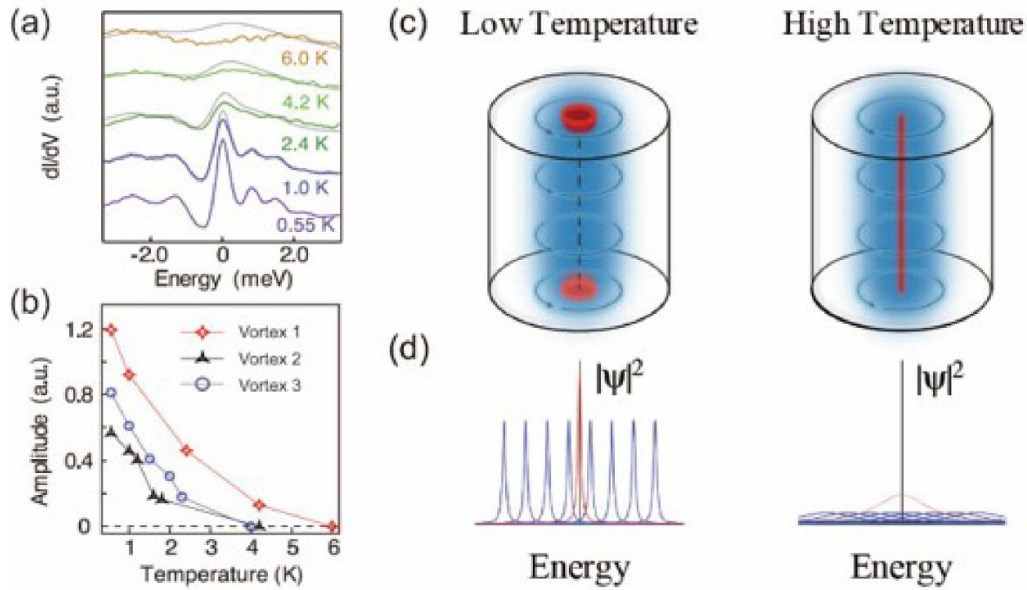


Figure 3. Temperature dependence of MBSs. (a) Temperature evolution of ZBP in a vortex core. The gray curves are numerically broadened 0.55 K data at each temperature. (b) Amplitude of the ZBPs in three vortices under different temperatures. The amplitude is defined as the peak valley difference of the ZBP. (c) Schematic of a vortex with a vertical magnetic field applied at low and high temperature. (d) Corresponding schematic of the energy-resolved bound states inside the vortex line. From [44]. Reprinted with permission from AAAS. All rights reserved.

due to intrinsic spin in the topological Dirac surface states [42, 67, 68]. As a result, the eigenvalues of the bound states follow an integer quantized sequence $E_\nu = \nu\Delta^2/E_F$ ($\nu = 0, \pm 1, \pm 2, \pm 3, \dots$). Therefore, the MZMs can then be seen as a special zero-energy CBS in a topological vortex [4].

3.3. Spatial pattern of the quantized states

The above discussion is supported by fitting the spatial distribution of the LDOSs of the CBSs using Fu–Kane Model [42, 44]. The excellent agreement between observed peak positions and calculated energy eigenvalues provides strong evidence for the topological nature of vortices in $\text{FeTe}_{0.55}\text{Se}_{0.45}$, demonstrating that the integer quantized CBS levels are the direct consequence of the topological surface states [61]. The calculated spatial patterns of the vortex bound states in two types of vortices are also consistent with the experimental observations (figures 7(c)–(h)), suggesting that the Dirac surface states contribute to the quasiparticle excitations of the topological vortices.

Therefore, the type of a vortex can be classified according to the nature of its electron states, either the Dirac surface states or conventional bulk bands. The intrinsic stoichiometric inhomogeneity [69–72] of $\text{FeTe}_{0.55}\text{Se}_{0.45}$ gives rise to the varying local electronic states across the sample surface, which will further influence the Dirac surface states. The Dirac surface states can be eliminated by either closing the bulk topological gap [73–75] or inducing an even number of topological band inversions at its time-reversal invariant momenta [76–78]. Both of them can occur locally in $\text{FeTe}_{0.55}\text{Se}_{0.45}$. This scenario naturally explains the question about the physical origin of the two types of vortices proposed in the last section.

Also, it provides stronger evidence of the topological nature of the observed MBS in $\text{FeTe}_{0.55}\text{Se}_{0.45}$.

4. Nearly quantized conductance plateau of MZM in $\text{FeTe}_{0.55}\text{Se}_{0.45}$

In the last two sections we focus on studying the energy levels of the in-gap states, demonstrating the existence of MZM in $\text{FeTe}_{0.55}\text{Se}_{0.45}$ and verified its topological nature. In this section, we will focus on the physical properties of the MZM itself and discuss the necessity of verifying the existence of MZMs. Theorists have predicted the quantized conductance plateau feature of the ZBP, which is regarded as a strong evidence for the existence of MZM. With sufficiently low temperature and strong tunnel coupling, the conductance of an MZM is proposed to show a quantized plateau at the value of $G_0 = 2e^2/h$, where e is the electron charge and h is the Planck's constant [79, 80]. This quantized Majorana conductance results from perfect resonant Andreev reflection [79–82] guaranteed by the inherent particle–hole symmetric nature of MZM [10].

$\text{FeTe}_{0.55}\text{Se}_{0.45}$ is chosen due to its large Δ/E_F ratio. The MZM is well separated from the CBSs, enable us to probe the intrinsic nature of the MZM without the contamination from other low-energy excitations. The experiment to study the Majorana conductance in vortex cores of $\text{FeTe}_{0.55}\text{Se}_{0.45}$ is carried out using an STM with extremely low effective electron temperature ($T_{\text{eff}} = 377$ mK) [45]. In order to achieve different tunnel coupling conditions, the tip-sample distance is precisely controlled over a large range by changing the tunnel-barrier conductance G_N ($G_N \equiv I_t/V_s$).

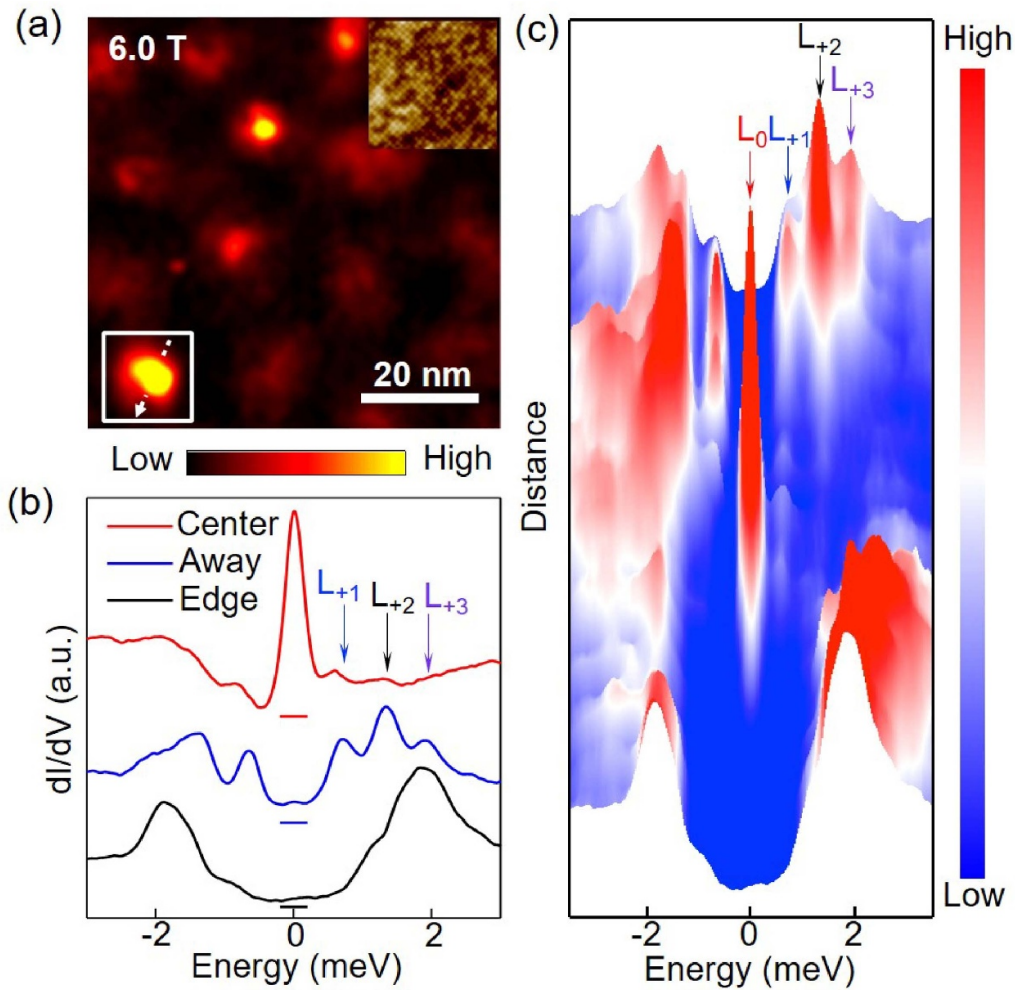


Figure 4. CBSs in a vortex with an MZM. (a) A normalized zero-bias conductance map measured at a magnetic field of 6.0 T. Inset: STM topography of FeTe_{0.55}Se_{0.45}. (b) Typical tunneling conductance spectra measured around the vortex marked by the white box in (a). (c) Three dimensional display of the line-cut intensity plot along the white dash line indicated in (a). Four sub-gap states are identified by the arrows in different colors. Reprinted by permission from Springer Nature Customer Service Centre GmbH: Springer Nature, Nature Physics [61] 2019. All rights reserved.

In a typical example of tunnel-coupling dependent measurement on a topological vortex [61], the ZBP remains a well-defined peak located at zero energy (figure 8(a)), and the zero-bias conductance saturates under a relatively high tunnel coupling (small tip-sample distance) condition (figure 8(d)). However, the conductance outside the superconducting gap increases monotonically as a function of G_N . This behavior is summarized in a three-dimensional (figure 8(b)) and a color-scale plot (figure 8(c)). In the experiment shown in figure 8, the plateau conductance (G_P) is equal to $0.64 G_0$ (figure 8(d)).

The conductance plateau in the tunnel-coupling dependent measurements is a unique character of MZMs, reflecting their intrinsic particle-hole symmetry. Other trivial states, including the normal states outside the superconductor gap and CBSs, increase monotonically with G_N without plateau feature. Figures 9(a)–(d) show the conductance behavior of CBSs in topological and ordinary vortices, and no plateau feature in the tunnel-coupling dependent measurement is observed. The measurement is also repeated at the same location at zero magnetic field (figures 9(e) and (f)). Both of the zero-bias

conductance and the high-bias conductance keep increasing as the tunnel coupling increases, ruling out the possibility of quantum ballistic transport [83–88]. All these observations verified that the conductance plateau feature is the unique character of MZMs in topological vortices, induced by the resonant Andreev reflection. The CBSs [55, 56] and other trivial states [89] do not have the particle-hole symmetry, showing an absence of a conductance plateau. The plateau behavior of ZBPs have been observed repeatedly in many stable topological vortices, but the plateau value varies from vortex to vortex. The plateau value smaller than G_0 is likely due to the instrumental broadening or the quasiparticle poisoning.

5. Other topologically non-trivial systems

5.1. Emerging topological edge states in buckled antimonene monolayers

Zhu *et al* reported the observation of topological edge states in antimonene monolayer epitaxially grown on Cu(111)

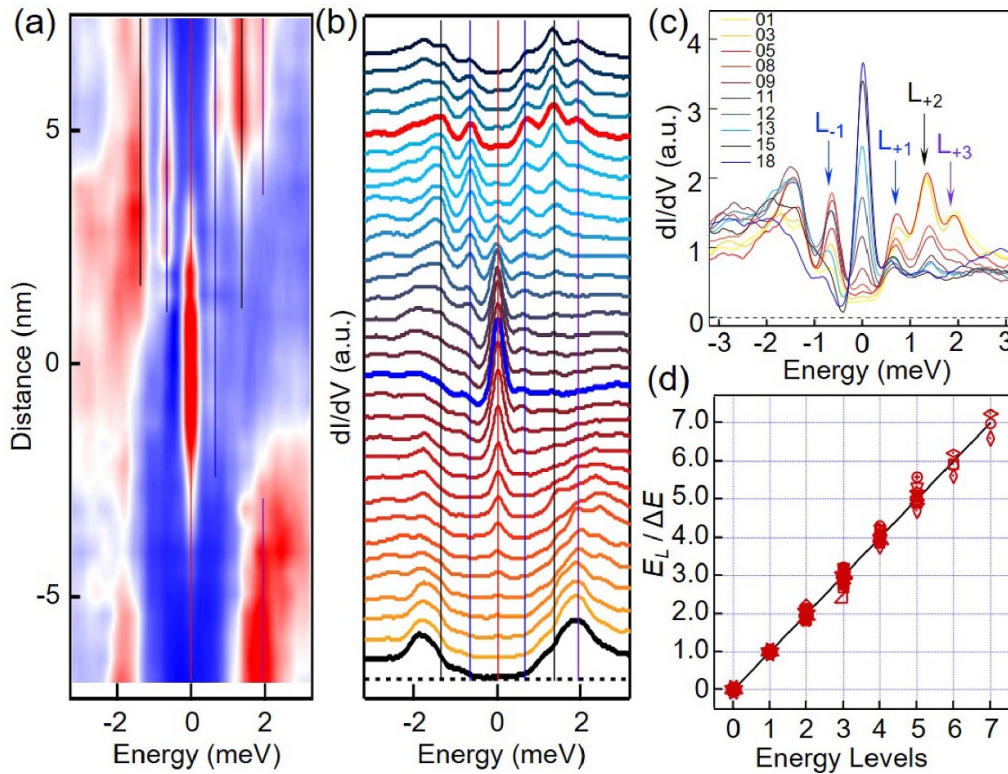


Figure 5. Integer quantized CBSs in a topological vortex. (a) A line-cut intensity plot of a topological vortex. (b) A waterfall-like plot of (a). (c) An overlapping plot of 10 dI/dV^{-1} spectra selected in (b). (d) Summary of $E_L/\Delta E$ vs level number data for seven different topological vortices. Reprinted by permission from Springer Nature Customer Service Centre GmbH: Springer Nature, Nature Physics [61] 2019. All rights reserved.

surface [90]. Figure 10(a) shows a typical antimonene island with hexagonal shape. Such island was fabricated on the first antimonene layer, which act as a buffer layer to screen the influence of the metal substrate on the edge electronic states of the island. The dI/dV spectrum measured at the center of the island shows the bulk state at the 1.68 eV, while the spectrum measured at the two opposite edges show edge states at 1.85 eV and 1.95 eV. The spatial evolution of the electronic structure is displayed in figures 10(c) and (d), showing the edge states arising from different bands with the bulk state. The result is also supported by density functional theory calculations, confirming the existence of topological edge states in antimonene monolayer. The topological edge states in bismuthene monolayer on SiC [91] and stanene on Cu(111) surface [92] are also reported. These novel two-dimensional topological materials demonstrated that the group-VA elemental thin films with strong SOC host topologically nontrivial states as excellent two-dimensional topological materials, opening opportunities for exploring two-dimensional topological physics and device applications.

5.2. Spontaneous formation of a superconductor-topological insulator-normal metal layered heterostructure

Wang *et al* reported the construction of a superconductor-topological insulator layered heterostructure [93]. The $\text{HfTe}_3/\text{HfTe}_5$ heterostructures were fabricated through

direct reaction and epitaxial growth of tellurium atoms on an $\text{Hf}(0001)$ substrate (figure 11(a)). In the a - c plane (figure 11(b)), an HfTe_5 layer can be considered as an HfTe_3 layer linked via Te-Te chains. In addition, the bond energy of the Te-Te chains in HfTe_5 is much weaker than that of the trigonal prismatic chains. So the Te-Te chains decompose much more easily than the Te-Hf keys. After the Te-Te chains decompose and the trigonal prismatic chains connect together one-by-one along the c direction, in principle, HfTe_5 layers should be turned into HfTe_3 layers. In experiment, the substrate was annealed to 530 ~ 590 centigrade, the topmost HfTe_5 layers of the sample transforms into HfTe_3 film due to some of the tellurium atoms escaping from the HfTe_5 layers at high temperature. As a result, an $\text{HfTe}_3/\text{HfTe}_5$ layered heterostructure are fabricated on the substrate.

The STS results under 4.2 K are shown in figures 11(c) and (d). The energy gap on the HfTe_5 surface is measured to be 60 meV (figure 11(d)). HfTe_5 films have been theoretically predicted as a promising large-gap topological insulator [94], and 60 meV is close to the bandgap for HfTe_5 with a thickness of three layers. The STS result on a HfTe_3 film show no gap feature under 4.2 K. However, under lower temperature of 0.45 K, a superconducting gap is clearly observed [93, 95]. Therefore, a superconductor-topological insulator layered heterostructure is fabricated by a simple tellurization method. This method opens up a route to fabricate heterostructures and nanodevices with a combination of multi-properties,

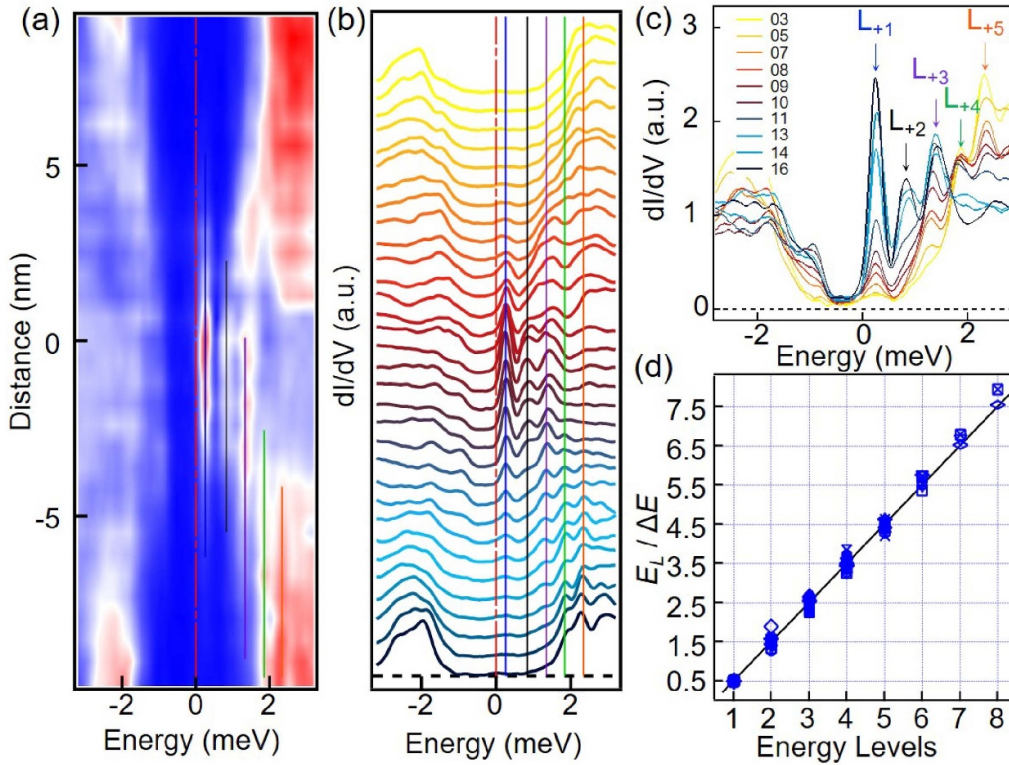


Figure 6. Half-odd-integer quantized CBSs in an ordinary vortex. (a) A line-cut intensity plot of an ordinary vortex. (b) A waterfall-like plot of (a). (c) An overlapping plot of 10 dI/dV^{-1} spectra selected in (b) with each energy level of the CBSs marked by L_{+1} , L_{+2} , L_{+3} , L_{+4} , and L_{+5} on the top. (d) Summary of $E_L/\Delta E$ vs level number data for different ordinary vortices. Reprinted by permission from Springer Nature Customer Service Centre GmbH: Springer Nature, Nature Physics [61] 2019. All rights reserved.

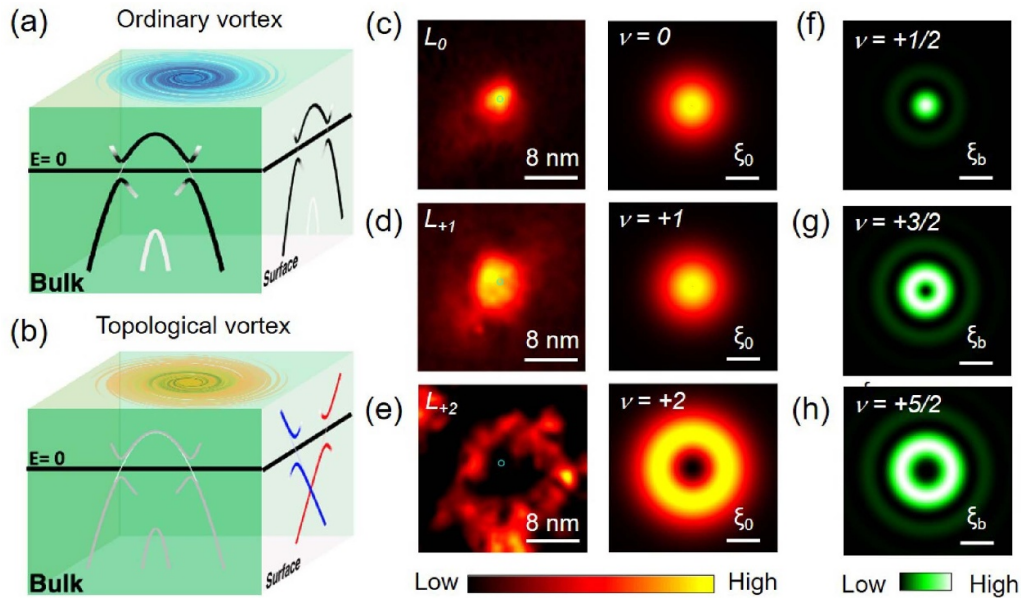


Figure 7. Spatial pattern of integer quantized CBSs. (a), (b) Schematic showing the difference between an ordinary vortex and a topological vortex. (c)–(e) Comparison plots between STM measurements and numerical calculations on a topological vortex. The 1st column is the conductance maps of each CBS level. The 2nd column shows numerical calculations of local density of states (LDOSs). (f)–(h) Numerical calculation on an ordinary vortex. Reprinted by permission from Springer Nature Customer Service Centre GmbH: Springer Nature, Nature Physics [61] 2019. All rights reserved.

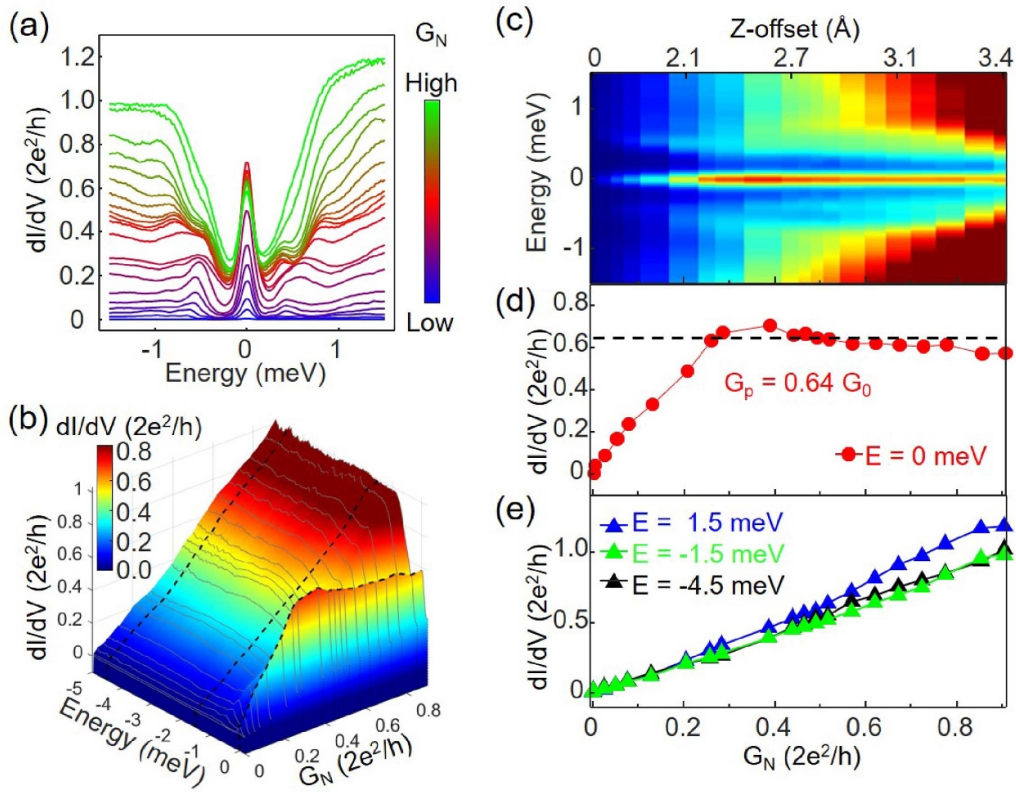


Figure 8. Zero-bias conductance plateau observed on $\text{FeTe}_{0.55}\text{Se}_{0.45}$. (a) An overlapping plot of dI/dV spectra under different tunnel coupling conditions. (b) A three-dimensional plot of tunnel coupling dependent measurement, $dI/dV(E, G_N)$. (c) A color-scale plot of (a). The z-offset information is provided on the upper axis. (d) A horizontal line-cut at the zero-bias from (c), showing a plateau behavior. (e) Horizontal line-cuts at high-bias values from (c). No plateau feature is seen. From [45]. Reprinted with permission from AAAS. All rights reserved.

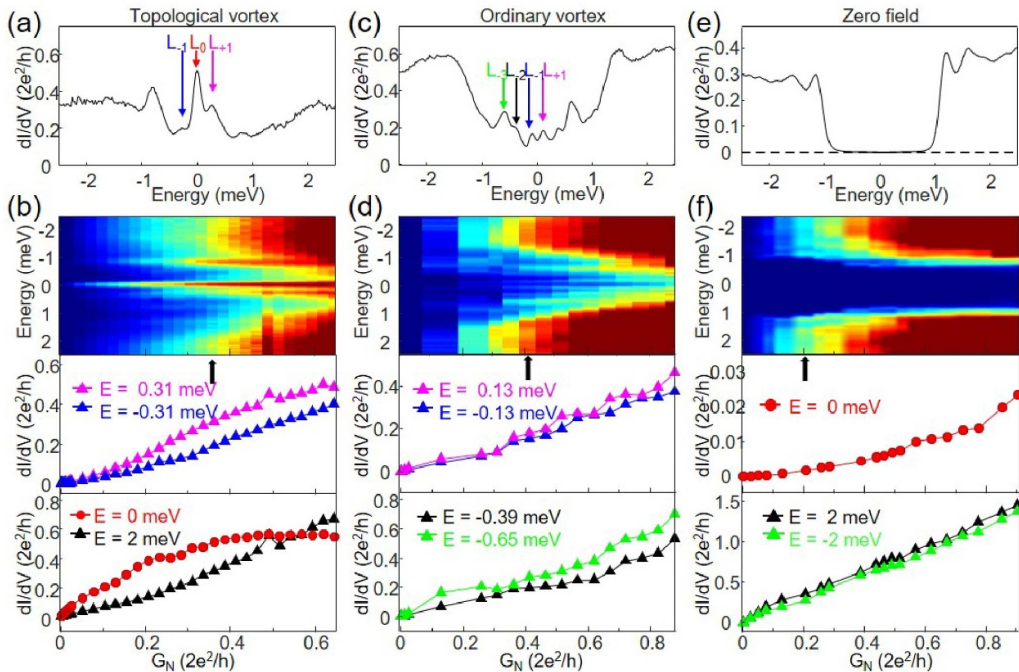


Figure 9. Majorana induced resonant Andreev reflection. (a) A dI/dV spectrum measured at the center of a topological vortex. (b) A tunnel coupling dependent measurement on the vortex of (a) at 2 T. Plateau feature is only observed at 0 meV. (c) A dI/dV spectrum measured at the center of an ordinary vortex. (d) A tunnel coupling dependent measurement on the vortex of (c) at 2 T. (e) A dI/dV spectrum measured at 0 T, showing a hard superconducting gap. (f) A tunnel coupling dependent measurement on the vortex of (e) at 0 T. From [45]. Reprinted with permission from AAAS. All rights reserved.

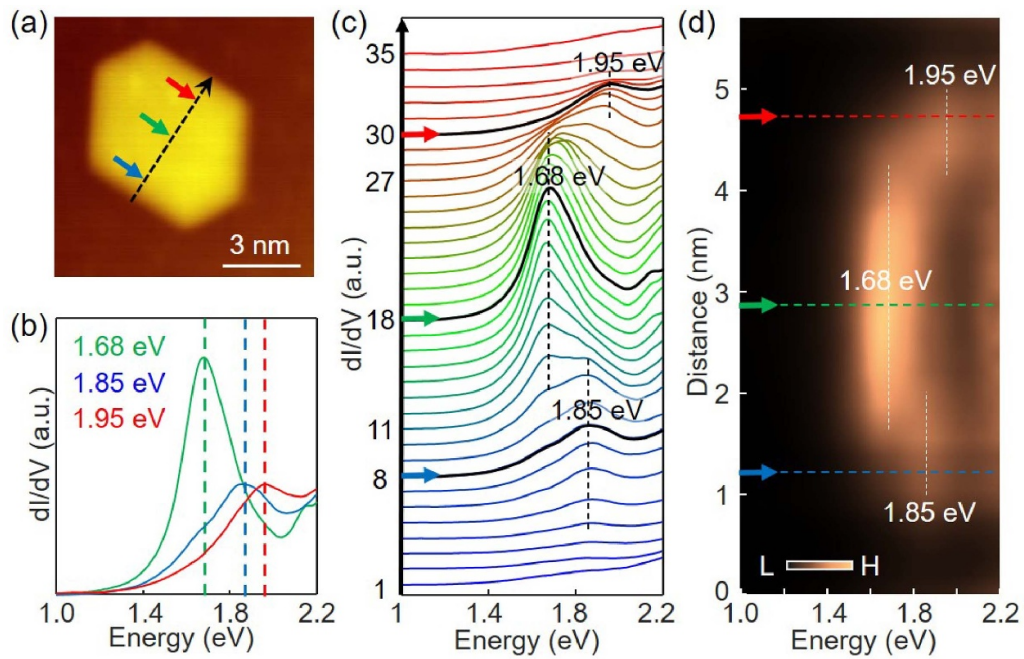


Figure 10. Experimental evidence for topological edge states. (a) STM topography of an antimonene island. (b) Three dI/dV curves measured at the different regions on the island in (a). (c) A waterfall-like plot of dI/dV curves along the black dashed arrow in (a). (d) The intensity plot of the spatially resolved measurement shown in (c). Reprinted with permission from [90]. Copyright 2019 American Chemical Society. All rights reserved.

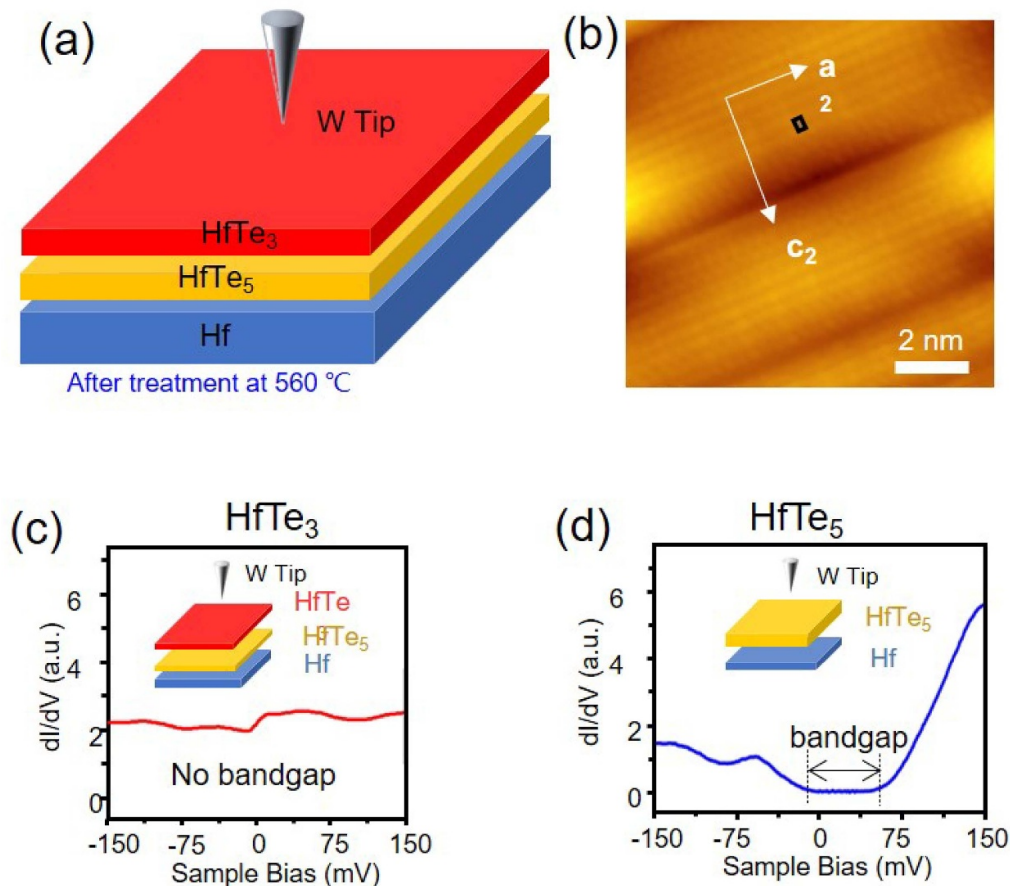


Figure 11. Structural and electronic properties of the as-grown $HfTe_3$ and $HfTe_5$ film. (a) Schematics of a tungsten tip located at the surface of $HfTe_3$ film. (b) Atomic-resolution STM image of the $HfTe_3$ film. (c) dI/dV spectrum taken on $HfTe_3$ surface. (d) dI/dV spectrum taken on $HfTe_5$ surface. [93] John Wiley & Sons. © 2016 WILEY-VCH Verlag GmbH & Co. KGaA, Weinheim. All rights reserved.

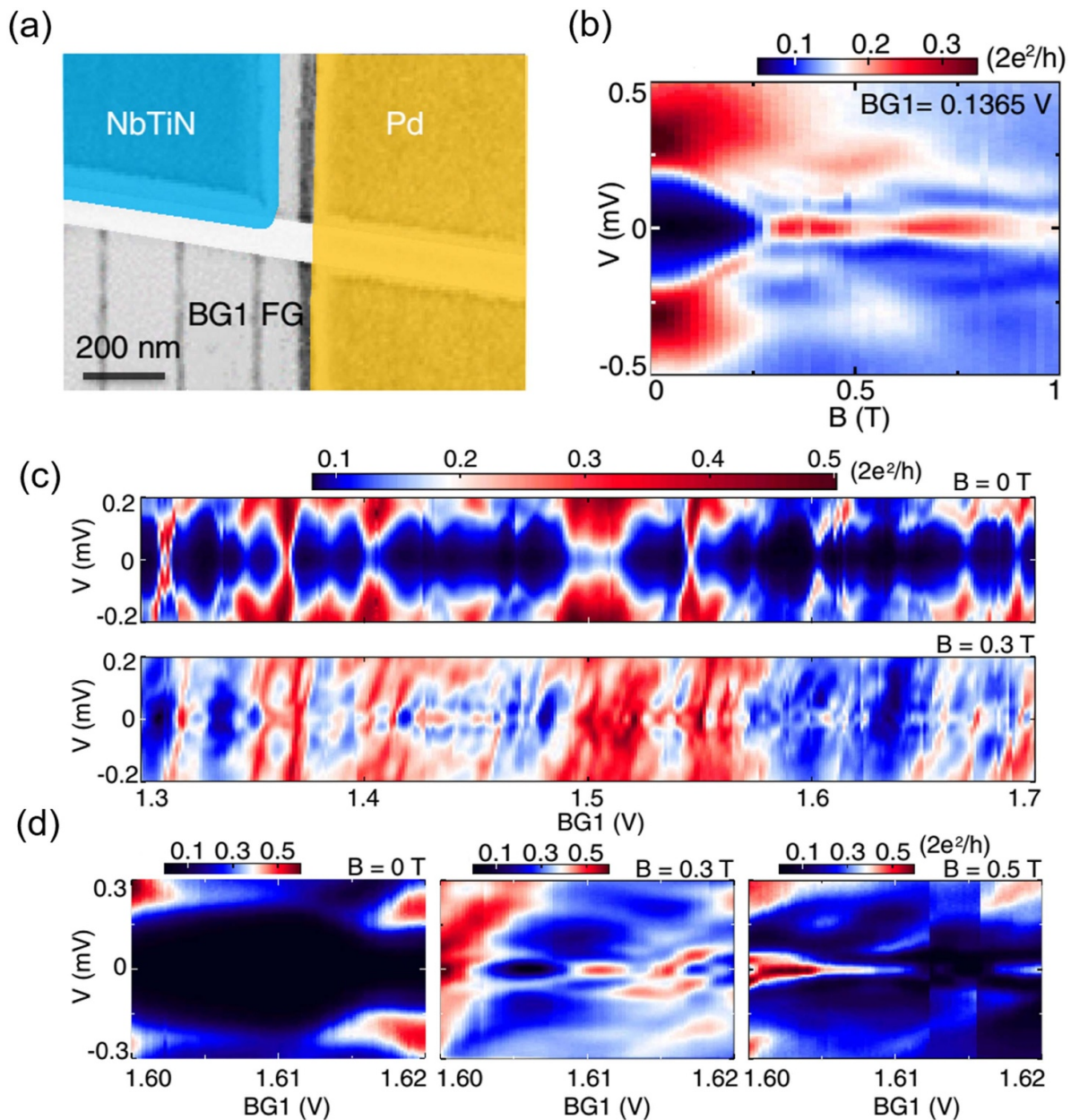


Figure 12. Non-Majorana ZBP in an InSb nanowire. (a) Scanning electron micrograph of the device. (b) Differential conductance maps in bias voltage V versus magnetic field at $BG1$ of -0.1365 V. ZBP is observed in a magnetic field range between 0.3 T and 1 T. (c) Differentiated conductance maps in bias voltage V versus $BG1$ at 0 T (upper panel) and 0.3 T (lower panel). (d) Differentiated conductance maps in bias voltage V versus $BG1$ at 0 (left panel), 0.3 (middle panel) and 0.5 T (right panel). Reprinted figure with permission from [96], Copyright 2019 by the American Physical Society. All rights reserved.

particularly to form systems to study Majorana quasiparticle excitations and topological quantum computation.

5.3. Non-Majorana states in proximitized nanowires and quantum anomalous Hall-superconductor devices

We would also like to bring the readers' attention to recent works, which shows that non-Majorana state could also show up as sharp ZBP or even give rise to conductance plateau. For example, Chen *et al* [96] observed ubiquitous non-Majorana ZBP instead of the predicted Majorana signal in certain limited parameter range. The chemical potential changes a lot

with the varying back-gate voltage, and an ubiquity in-gap state can be observed in this measurement (figure 10), which was assigned to the signal of Andreev bound states (ABSs). Those ABSs show ZBP features when applying a finite magnetic field (figures 12(c) and (d)). Yu *et al* [97] fabricated three-terminal InSb nanowire devices in the Majorana configuration, which can independently detect the signal of both nanowire ends. The experimental results show nearly quantized ZBP on the left side and absence of ZBP on the right side (figure 13), demonstrating the possibility of non-Majorana signal in this Majorana configuration. Kayyalha *et al* [98] reported the appearance of trivial half-quantized two-terminal

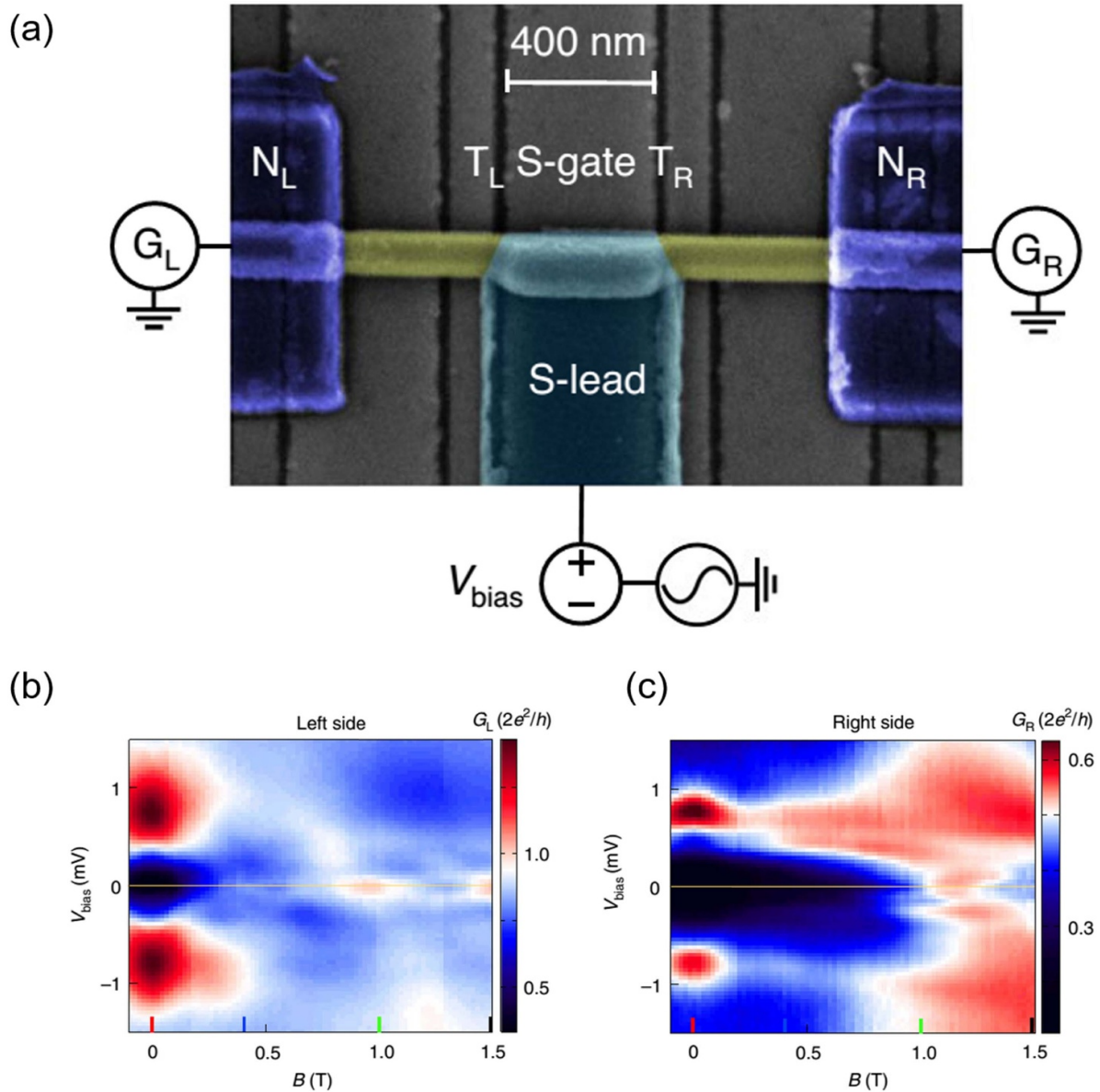


Figure 13. Different electronic states at the two ends of a nanowire. (a) Three-terminal nanowire device. (b), (c) Differential conductance maps in bias voltage V versus magnetic field at the two ends of the device. Reproduced with permission from [97]. (insert copyright line, if specified). All rights reserved.

conductance plateau when the SC layer is strongly coupled to the QAH sample (figure 14). The results show that the half-quantized conductance plateaus in these QAH-SC hybrid devices is unlikely to be induced by chiral Majorana fermions.

These works set up high requirements to the community on careful analysis of their experimental data concerning Majorana states. An intuitive connection between the ZBP or plateau feature to Majorana physics should always be avoided, since other trivial states could behave in a similar manner. The conclusion should be drawn with great caution.

6. Summary and perspective

In this topic review, we present an overview of the recent progress of STM studies on exploring the MBSs, typically

in iron-based superconductor $\text{FeTe}_{0.55}\text{Se}_{0.45}$. The observed ZBP in the center of the vortex of $\text{FeTe}_{0.55}\text{Se}_{0.45}$ is verified as MBSs. Thanks to the high T_c and the large Δ/E_F ratio of $\text{FeTe}_{0.55}\text{Se}_{0.45}$, it proves to be a good platform to study the intrinsic physical properties of the Majorana modes. To that, the topological nature of the vortices hosting MZM is reviewed and discussed. Moreover, the spectral weight of the zero mode shows quantized conductance plateau behavior in the tunnel-coupling dependent STM measurements, giving strong evidence of the existence of MZMs in $\text{FeTe}_{0.55}\text{Se}_{0.45}$.

In addition, the layered heterojunction interfaces of superconductors and topological insulators also bring exciting results and huge potential on the Majorana research. In recent years, different 2D superconducting materials and

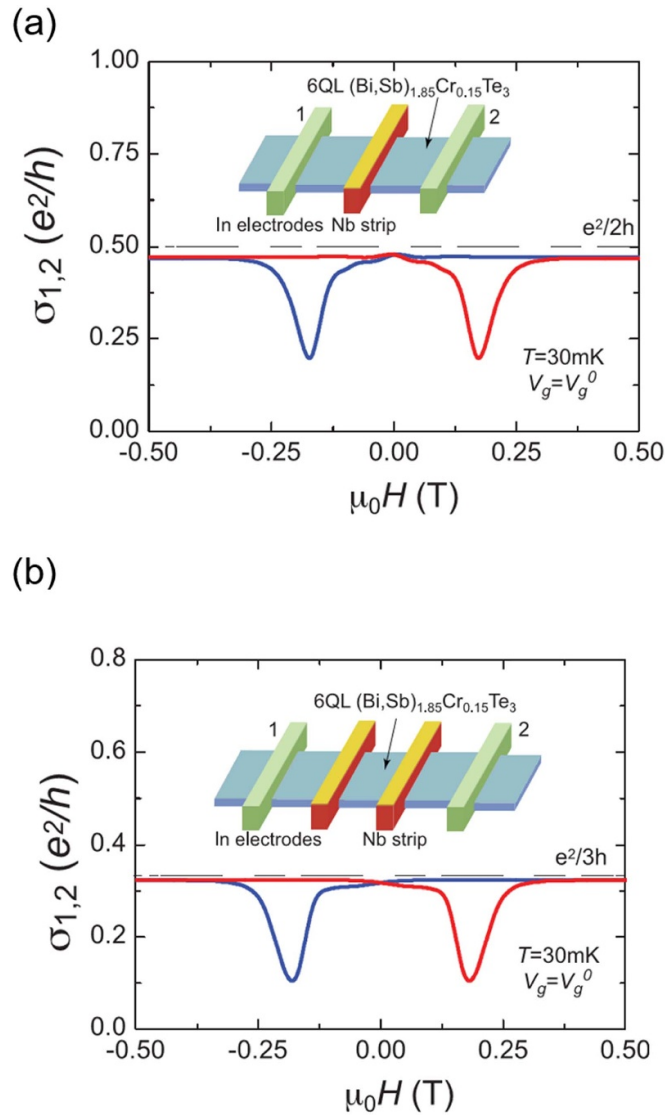


Figure 14. Two-terminal conductance in 6QL uniformly doped QAH-Nb strip devices. (a) $\mu_0 H$ dependence of $\sigma_{1,2}$ measured across one Nb strip. (b) Same as (a) for two Nb strips. From [98]. Reprinted with permission from AAAS. All rights reserved.

topological materials have been discovered. The rich and flexible combinations of these new materials provide a large library from which we can design different types of promising platforms for exploring the MBSs as well as future fault-tolerant quantum computing.

However, there is still a long way to experimentally realize the topological quantum computing. In fact, the braiding of two MZMs carried by vortices is still a challenging task and several problems need to be overcome. First of all, braiding of two MZMs requires controlled movement of vortices by STM tip (figure 15). In a typical scanning probe microscopy setup, the vortices can be driven by magnetic force [99], local heating [100], local contact [101] and so on. However, the controlled driving of vortex motion usually requires special design or modification of the tip end, which would compromise the spatial and energy resolution of STM, and thus impair the capability to detect quantum information in MBSs. Secondly, the

braiding process requires stable and robust MZM inside the vortex during its movement. As has been discussed, the surface of $\text{FeTe}_{0.55}\text{Se}_{0.45}$ is inhomogeneous and has topological and non-topological regions. If the vortex is moved into the non-topological region, the MZM would disappear. As a result, new materials with more homogeneous electronic structure for more robust MZMs have to be explored. Thirdly, theoretical proposals on how to design the braiding experiment and what quantities to measure by the STM tip are needed [60, 102].

As a result, new Majorana platforms with more homogeneous bulk and surface electronic structure have to be explored [54]. New materials with higher homogeneity would serve as more practical platforms in manipulating the vortices containing MBS. Appropriate theoretical proposal as well as experimental design will also be critical in realizing the braiding of the MBSs in the future.

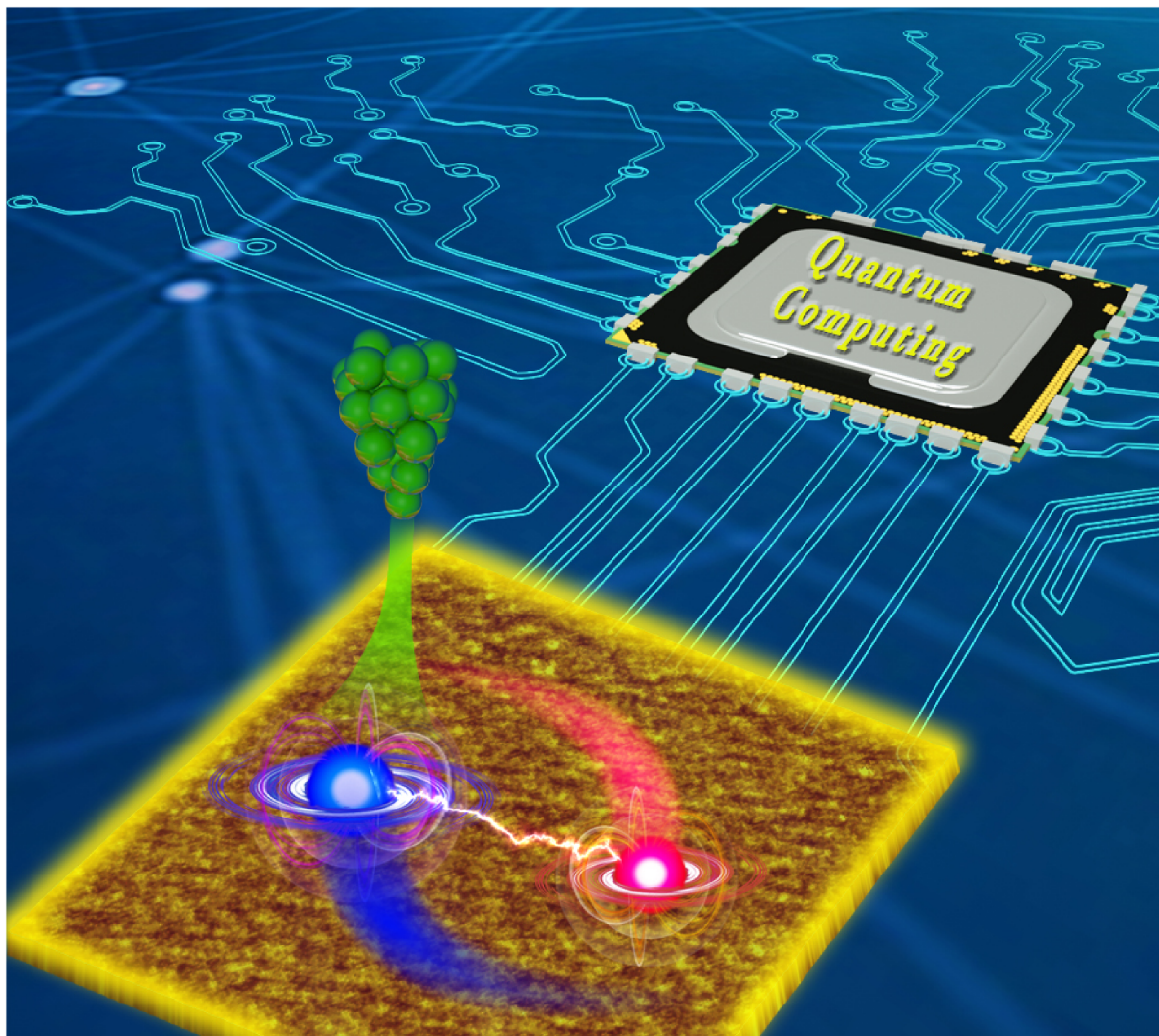


Figure 15. Schematic showing the manipulation of topological vortices using a tip.




Data availability statement

No new data were created or analyzed in this study.

Acknowledgments

The work is supported by grants from the Ministry of Science and Technology of China (2019YFA0308500, 2018YFA0305800, and 2016YFA0202300), the National Natural Science Foundation of China (61888102, 51991340, and 52072401), and the Chinese Academy of Sciences (XDB28000000 and XDB30000000).

ORCID iDs

Geng Li  <https://orcid.org/0000-0002-3347-7222>
 Shiyu Zhu  <https://orcid.org/0000-0002-8771-5273>
 Hong-Jun Gao  <https://orcid.org/0000-0002-2088-0522>

References

- [1] Majorana E 1937 *Nuovo Ciment.* **14** 171
- [2] Wilczek F 2009 *Nat. Phys.* **5** 614
- [3] Qi X L and Zhang S C 2011 *Rev. Mod. Phys.* **83** 1057
- [4] Alicea J 2012 *Rep. Prog. Phys.* **75** 076501
- [5] Ivanov D A 2001 *Phys. Rev. Lett.* **86** 268
- [6] Bravyi S 2006 *Phys. Rev. A* **73** 042313
- [7] Kitaev A Y 2003 *Ann. Phys.* **303** 2
- [8] Beenakker C W J 2013 *Annu. Rev. Condens. Matter Phys.* **4** 113
- [9] Bi D, Yang X, Marchetti M C and Manning M L 2016 *Phys. Rev. X* **6** 031016
- [10] Nayak C, Simon S H, Stern A, Freedman M and Das Sarma S 2008 *Rev. Mod. Phys.* **80** 1083
- [11] Moore G and Read N 1991 *Nucl. Phys. B* **360** 362
- [12] Read N and Green D 2000 *Phys. Rev. B* **61** 10267
- [13] Kitaev A Y 2001 *Phys. Uspekhi.* **44** 131
- [14] Jeon S, Xie Y L, Li J, Wang Z J, Bernevig B A and Yazdani A 2017 *Science* **358** 772
- [15] Lutchyn R M, Sau J D and Das Sarma S 2010 *Phys. Rev. Lett.* **105** 077001
- [16] Sau J D, Lutchyn R M, Tewari S and Das Sarma S 2010 *Phys. Rev. Lett.* **104** 040502

- [17] Nadj-Perge S, Drozdov I K, Bernevig B A and Yazdani A 2013 *Phys. Rev. B* **88** 020407
- [18] Braunecker B and Simon P 2013 *Phys. Rev. Lett.* **111** 147202
- [19] Klinovaja J, Stano P, Yazdani A and Loss D 2013 *Phys. Rev. Lett.* **111** 186805
- [20] Vazifeh M M and Franz M 2013 *Phys. Rev. Lett.* **111** 206802
- [21] Li J, Neupert T, Wang Z J, MacDonald A H, Yazdani A and Bernevig B A 2016 *Nat. Commun.* **7** 12297
- [22] Pientka F, Keselman A, Berg E, Yacoby A, Stern A and Halperin B I 2017 *Phys. Rev. X* **7** 021032
- [23] Mourik V, Zuo K, Frolov S M, Plissard S R, Bakkers E P A M and Kouwenhoven L P 2012 *Science* **336** 1003
- [24] Deng M T, Yu C L, Huang G Y, Larsson M, Caroff P and Xu H Q 2012 *Nano Lett.* **12** 6414
- [25] Churchill H O H, Fatemi V, Grove-Rasmussen K, Deng M T, Caroff P, Xu H Q and Marcus C M 2013 *Phys. Rev. B* **87** 241401
- [26] Deng M T, Vaitiekėnas S, Hansen E B, Danon J, Leijnse M, Flensberg K, Nygard J, Krogstrup P and Marcus C M 2016 *Science* **354** 1557
- [27] Lutchyn R M, Bakkers E P A M, Kouwenhoven L P, Krogstrup P, Marcus C M and Oreg Y 2018 *Nat. Rev. Mater.* **3** 52
- [28] Nadj-Perge S, Drozdov I K, Li J, Chen H, Jeon S, Seo J, MacDonald A H, Bernevig B A and Yazdani A 2014 *Science* **346** 602
- [29] Kim H, Palacio-Morales A, Posske T, Rozsa L, Palotas K, Szunyogh L, Thorwart M and Wiesendanger R 2018 *Sci. Adv.* **4** eaar5251
- [30] Ruby M, Pientka F, Peng Y, von Oppen F, Heinrich B W and Franke K J 2015 *Phys. Rev. Lett.* **115** 197204
- [31] Ruby M, Heinrich B W, Peng Y, von Oppen F and Franke K J 2017 *Nano Lett.* **17** 4473
- [32] Wei P, Manna S, Eich M, Lee P and Moodera J 2019 *Phys. Rev. Lett.* **122** 247002
- [33] Manna S, Wei P, Xie Y M, Law K T, Lee P A and Moodera J S 2020 *Proc. Natl Acad. Sci. USA* **117** 8775
- [34] Fornieri A *et al* 2019 *Nature* **569** 89
- [35] Ren H C *et al* 2019 *Nature* **569** 93
- [36] Xu J P *et al* 2015 *Phys. Rev. Lett.* **114** 017001
- [37] Sun H H *et al* 2016 *Phys. Rev. Lett.* **116** 257003
- [38] Menard G C, Guissart S, Brun C, Leriche R T, Trif M, Debontridder F, Demaille D, Roditchev D, Simon P and Cren T 2017 *Nat. Commun.* **8** 2040
- [39] Palacio-Morales A, Mascot E, Cocklin S, Kim H, Rachel S, Morr D K and Wiesendanger R 2019 *Sci. Adv.* **5** eaav6600
- [40] Kezilebieke S, Huda M N, Vano V, Aapro M, Ganguli S C, Silveira O J, Glodzik S, Foster A S, Ojanen T and Liljeroth P 2020 *Nature* **588** 424
- [41] Zhang P *et al* 2018 *Science* **360** 182
- [42] Fu L and Kane C L 2008 *Phys. Rev. Lett.* **100** 096407
- [43] Hao N and Hu J P 2019 *Natl Sci. Rev.* **6** 213
- [44] Wang D *et al* 2018 *Science* **362** 333
- [45] Zhu S *et al* 2020 *Science* **367** 189
- [46] Wang Z Y, Rodriguez J O, Jiao L, Howard S, Graham M, Gu G D, Hughes T L, Morr D K and Madhavan V 2020 *Science* **367** 104
- [47] Chen C, Jiang K, Zhang Y, Liu C F, Liu Y, Wang Z Q and Wang J 2020 *Nat. Phys.* **16** 536
- [48] Liu Q *et al* 2018 *Phys. Rev. X* **8** 041056
- [49] Wang Z J *et al* 2015 *Phys. Rev. B* **92** 115119
- [50] Xu G, Lian B, Tang P Z, Qi X-L and Zhang S-C 2016 *Phys. Rev. Lett.* **117** 047001
- [51] Chen M Y, Chen X Y, Yang H, Du Z Y, Zhu X Y, Wang E Y and Wen H-H 2018 *Nat. Commun.* **9** 970
- [52] Borisenko S, Bezguba V, Fedorov A, Kushnirenko Y, Voroshnin V, Sturza M, Aswartham S and Yaresko A 2020 *npj Quantum Mater.* **5** 67
- [53] Mascot E, Cocklin S, Graham M, Mashkooori M, Rachel S and Morr D K 2021 (arXiv:2102.05116)
- [54] Liu W Y *et al* 2020 *Nat. Commun.* **11** 5688
- [55] Caroli C, de Gennes P G and Matricon J 1964 *Phys. Lett.* **9** 307
- [56] Hess H F, Robinson R B and Waszczak J V 1990 *Phys. Rev. Lett.* **64** 2711
- [57] Hosur P, Ghaemi P, Mong R S K and Vishwanath A 2011 *Phys. Rev. Lett.* **107** 097001
- [58] Hung H-H, Ghaemi P, Hughes T L and Gilbert M J 2013 *Phys. Rev. B* **87** 035401
- [59] Machida T, Sun Y, Pyon S, Takeda S, Kohsaka Y, Hanaguri T, Sasagawa T and Tamegai T 2019 *Nat. Mater.* **18** 811
- [60] Chiu C K, Machida T, Huang Y Y, Hanaguri T and Zhang F C 2020 *Sci. Adv.* **6** eaay0443
- [61] Kong L *et al* 2019 *Nat. Phys.* **15** 1181
- [62] Rinott S, Chashka K B, Ribak A, Rienks E D L, Taleb-Ibrahimi A, Le Fevre P, Bertran F, Randeria M and Kanigel A 2017 *Sci. Adv.* **3** e1602372
- [63] Hayashi N, Isoshima T, Ichioka M and Machida K 1998 *Phys. Rev. Lett.* **80** 2921
- [64] Shan L *et al* 2011 *Nat. Phys.* **7** 325
- [65] Hanaguri T, Kitagawa K, Matsubayashi K, Mazaki Y, Uwatoko Y and Takagi H 2012 *Phys. Rev. B* **85** 214505
- [66] Gygi F and Schluter M 1991 *Phys. Rev. B* **43** 7609
- [67] Khaymovich I M, Kopnin N B, Mel'nikov A S and Shereshevskii I A 2009 *Phys. Rev. B* **79** 224506
- [68] Hu L-H, Li C, Xu D-H, Zhou Y and Zhang F-C 2016 *Phys. Rev. B* **94** 224501
- [69] He X, Li G, Zhang J, Karki A B, Jin R, Sales B C, Sefat A S, McGuire M A, Mandrus D and Plummer E W 2011 *Phys. Rev. B* **83** 220502
- [70] Lin W, Li Q, Sales B C, Jesse S, Sefat A S, Kalinin S V and Pan M 2013 *ACS Nano* **7** 2634
- [71] Singh U R, White S C, Schmaus S, Tsurkan V, Loidl A, Deisenhofer J and Wahl P 2013 *Phys. Rev. B* **88** 155124
- [72] Massee F, Sprau P O, Wang Y L, Davis J C, Ghigo G, Gu G D and Kwok W K 2015 *Sci. Adv.* **1** e1500033
- [73] Hasan M Z and Kane C L 2010 *Rev. Mod. Phys.* **82** 3045
- [74] Schubert G, Fehske H, Fritz L and Vojta M 2012 *Phys. Rev. B* **85** 201105
- [75] Sacksteder V, Ohtsuki T and Kobayashi K 2015 *Phys. Rev. Appl.* **3** 064006
- [76] Fu L, Kane C L and Mele E J 2007 *Phys. Rev. Lett.* **98** 106803
- [77] Noguchi R *et al* 2019 *Nature* **566** 518
- [78] Qin S, Hu L, Wu X, Dai X, Fang C, Zhang F-C and Hu J 2019 *Sci. Bull.* **64** 1207
- [79] Law K T, Lee P A and Ng T K 2009 *Phys. Rev. Lett.* **103** 237001
- [80] Wimmer M, Akhmerov A R, Dahlhaus J P and Beenakker C W J 2011 *New J. Phys.* **13** 053016
- [81] Flensberg K 2010 *Phys. Rev. B* **82** 180516
- [82] Setiawan F, Liu C X, Sau J D and Das Sarma S 2017 *Phys. Rev. B* **96** 184520
- [83] Beenakker C W 1992 *Phys. Rev. B* **46** 12841
- [84] Gul Ö *et al* 2018 *Nat. Nanotechnol.* **13** 192
- [85] Kammhuber J *et al* 2016 *Nano Lett.* **16** 3482
- [86] Kjaergaard M *et al* 2016 *Nat. Commun.* **7** 12841
- [87] van Wees B J, van Houten H, Beenakker C W, Williamson J G, Kouwenhoven L P, van der Marel D and Foxon C T 1988 *Phys. Rev. Lett.* **60** 848
- [88] Zhang H *et al* 2017 *Nat. Commun.* **8** 16025
- [89] Liu C X, Sau J D, Stanescu T D and Das Sarma S 2017 *Phys. Rev. B* **96** 075161
- [90] Zhu S-Y *et al* 2019 *Nano Lett.* **19** 6323
- [91] Reis F, Li G, Dudy L, Bauernfeind M, Glass S, Hanke W, Thomale R, Schäfer J and Claessen R 2017 *Science* **357** 287
- [92] Deng J *et al* 2018 *Nat. Mater.* **17** 1081

- [93] Wang Y-Q *et al* 2016 *Adv. Mater.* **28** 5013
- [94] Weng H M, Dai X and Fang Z 2014 *Phys. Rev. X* **4** 011002
- [95] Felser C, Finckh E W, Kleinke H, Rucker F and Tremel W 1998 *J. Mater. Chem.* **8** 1787
- [96] Chen J, Woods B D, Yu P, Hocevar M, Car D, Plissard S R, Bakkers E P A M, Stanescu T D and Frolov S M 2019 *Phys. Rev. Lett.* **123** 107703
- [97] Yu P, Chen J, Gomanko M, Badawy G, Bakkers E P A M, Zuo K, Mourik V and Frolov S M 2021 *Nat. Phys.* **17** 482
- [98] Kayyalha M *et al* 2020 *Science* **367** 64
- [99] Auslaender O M, Luan L, Straver E W J, Hoffman J E, Koshnick N C, Zeldov E, Bonn D A, Liang R X, Hardy W N and Moler K A 2009 *Nat. Phys.* **5** 35
- [100] Ge J Y, Gladilin V N, Tempere J, Xue C, Devreese J T, Van de Vondel J, Zhou Y H and Moshchalkov V V 2016 *Nat. Commun.* **7** 13880
- [101] Kremen A, Wissberg S, Haham N, Persky E, Frenkel Y and Kalisky B 2016 *Nano Lett.* **16** 1626
- [102] Liu C X, Liu D E, Zhang F C and Chiu C K 2019 *Phys. Rev. Appl.* **12** 054035